Geophysical Research Letters

RESEARCH LETTER
10.1029/2022GL098744

Argo Reveals the Scales and Provenance of Equatorial Island Upwelling Systems

Kristopher B. Karnauskas[1,2] and Donata Giglio[1]

[1]Department of Atmospheric and Oceanic Sciences, University of Colorado Boulder, Boulder, CO, USA, [2]Cooperative Institute for Research in Environmental Sciences, University of Colorado Boulder, Boulder, CO, USA

Key Points:

- Twenty-two years of Argo profiles reveal the localized topographic upwelling signal west of the two equatorial archipelagos
- The observed thickening of the thermocline west of the Galápagos is associated with the localized mean upwelling velocity of 12 m per day
- The blockage of the equatorial undercurrent by islands contributes to the productivity of waters west of the equatorial archipelagos

Supporting Information:

Supporting Information may be found in the online version of this article.

Correspondence to:

K. B. Karnauskas,
kristopher.karnauskas@colorado.edu

Citation:

Karnauskas, K. B., & Giglio, D. (2022). Argo reveals the scales and provenance of equatorial island upwelling systems. *Geophysical Research Letters*, *49*, e2022GL098744. https://doi.org/10.1029/2022GL098744

Received 17 MAR 2022
Accepted 15 AUG 2022

Abstract Equatorial islands have distinct oceanographic signatures, including cool sea surface temperature and high productivity immediately to their west. It has long been hypothesized that topographic upwelling is responsible for such characteristics—upward deflection by the islands of the eastward-flowing equatorial undercurrent (EUC). Using 22 years of in situ measurements by Argo, we provide the first direct observations of this process occurring with consistency at two prominent archipelagos in the equatorial Pacific. Argo measurements resolve a clear subsurface thermal fingerprint of vertical divergence at the depth of the EUC, confined to within 100 km of both the Gilbert (∼175°E) and Galápagos Islands (∼90°W). This signal at the Galápagos is well-reproduced by a high-resolution ocean reanalysis, enabling the estimation of vertical velocities balancing the zonal convergence of the EUC upon the islands. This sharpened view of the physics underpinning such important tropical ecosystems has implications for strategies to model and predict them.

Plain Language Summary Upwelling fuels marine life by bringing nutrient-rich water into the sunlit surface layer. Upwelling can also impact the atmosphere, because the water brought to the surface is colder, which affects the wind and clouds. The surprising abundance and diversity of life—from corals to fish to seabirds—around equatorial islands are thought to be caused by a unique form of upwelling. A global array of thousands of floats called Argo is used to reveal the structure of this unique form of upwelling. Unlike most upwelling zones (e.g., California), which are driven directly by the wind combined with Earth's rotation, upwelling at equatorial islands is shown here to be due to a massive underwater current that flows along the equator colliding with the islands. The results are corroborated with a high-resolution model and recent data from underwater gliders near the Galápagos. These insights have immediate implications for predictions of how such important tropical ecosystems will change in the future.

1. Introduction

Upwelling is a ubiquitous feature of the equatorial ocean, as easterly trade winds drive poleward Ekman transport on either side of the equator (Cromwell, 1953; Ekman, 1905). While vertical ocean velocities are prohibitively slow to measure directly, their crucial role in fueling primary productivity, driving air-sea carbon flux, cooling the sea surface, and modulating the coupled ocean-atmosphere system has long been recognized (Bjerknes, 1969; Field et al., 1998). One analysis of shipboard observations in the Pacific during the 1990s estimated peak equatorial upwelling at 0.9–2.4 m per day (Johnson et al., 2001)—roughly consistent with earlier estimates ranging from 1.0 m day^{-1} (Wyrtki, 1981) to 2.5 m day^{-1} (Bryden & Brady, 1985). These values describe the large-scale upwelling velocity in the *open* equatorial ocean.

Amid this broad stretch of upwelling across the equatorial Pacific commonly referred to as the "cold tongue" are several islands and the archipelagos with markedly stronger signals of cool sea surface temperature (SST) and high productivity. Found immediately west of the Gilbert and Galápagos Islands are localized enhancements of the surface characteristics of the cold tongue (Figure 1). For example, to the west of Isla Isabela, the Galápagos in the eastern equatorial Pacific has a further SST reduction by 2°C and an order of magnitude higher surface chlorophyll concentration. At the Gilbert Islands in the western Pacific, the signals are roughly −0.2°C in SST and doubling of chlorophyll—smaller but nonetheless clearly evident in satellite observations. The same phenomenon has been documented at islands as small as Jarvis Island (0.4°S, 160°W, and 4.5 km^2) with in situ measurements (Gove et al., 2006; Hendry & Wunsch, 1973; Karnauskas et al., 2016). These surface oceanographic patterns thus appear common to islands and archipelagos near the equator, regardless of their size or arrangement.

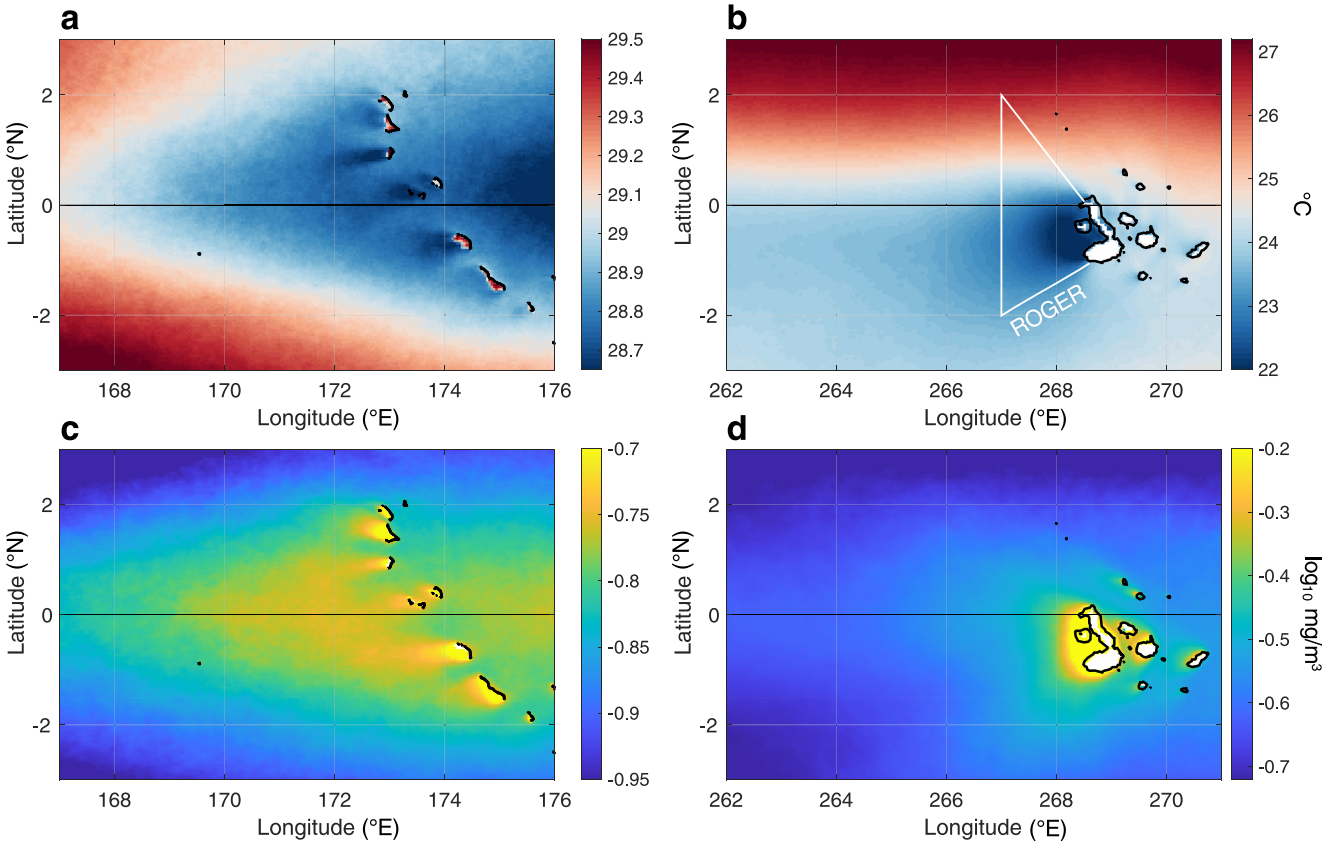

Figure 1. Surface signatures of equatorial island upwelling systems. Sea surface temperature (°C) in the vicinity of the (a) Gilbert and (b) Galápagos Islands from Moderate Resolution Imaging Spectroradiometer (4-km resolution, entire mission composite, and average of products from Terra and Aqua). The white trapezoid in panel (b) denotes the sampling pattern of the Repeat Observations by Gliders in the Equatorial Region glider campaign referred to in the main text. (c, d) As in panels (a and b) but for the log of surface chlorophyll-*a* concentration. To facilitate the comparison of spatial scales, each panel encompasses the same area (9° longitude by 6° latitude). (b, d) To visualize features of interest, color axes span wider ranges of values for the Galápagos Islands.

While the spatial scale of equatorial island signals is much smaller than that of the basin-scale cold tongue, they are significant for several reasons. Equatorial islands and archipelagos such as the aforementioned are hotspots of life compared to the expanse of open ocean between the Maritime Continent and mainland South America. The distribution and composition of coral reefs, the habitats of plankton and animals, the structure of fisheries, and the marine ecosystems as a whole are closely linked to the patterns of SST and chlorophyll evident in Figure 1 (Cannon et al., 2021; Feldman et al., 1984; Gove, 2005; Houvenaghel, 1978; Karnauskas et al., 2015; Pauly & Christensen, 1995; Vargas et al., 2005). Indeed, biodiversity and important societal dimensions, such as economies and food security are tied to these oceanographic patterns and their variability. Additionally, given their chance location on the equator, the Galápagos and Gilbert Islands, through their impacts on ocean temperature, salinity, and circulation, may not be trivial features of the climate. The Galápagos enhances the zonal SST gradient at the initiation of the cold tongue in the eastern Pacific, and the Gilberts serve to extend the productive cold tongue by hundreds of kilometers at its terminus near the dateline (Karnauskas & Cohen, 2012). Modeling studies have shown acute sensitivities of the basin-scale oceanography and climate dynamics to the presence of the Galápagos (Eden & Timmermann, 2004; Karnauskas et al., 2007, 2008) and Gilbert Islands (Karnauskas et al., 2017).

Our ability to model and predict the variability of these climatic punctuation marks, and protect the vital marine ecosystems within them, is limited by our understanding of their underlying physical mechanism. One hypothesis to explain the exceptionally cool and productive waters observed immediately west of the equatorial islands involves the encounter of a subsurface current with topography, which satisfies continuity by deflecting some fraction of the water toward the surface, thus cooling SST by vertical temperature advection and enhancing chlorophyll by delivering nutrients to the euphotic zone. In this case, the subsurface current is the eastward-flowing

equatorial undercurrent (EUC), naturally constrained to the equator by the Coriolis force, and the topography is provided by the steep bathymetry of the Gilbert and Galápagos Islands. The dynamics underpinning this phenomenon may be similar to those described by Hendry and Wunsch (1973), following Drazin (1961), who invoked the Bernoulli principle to explain the vertical isotherm displacements and the steady, inviscid flow that follows them. Remarkably, this hypothesis was also inferred—albeit qualitatively—and linked to the chemical and biological patterns by the Belgian biologist, Guy Thomas Houvenaghel, from a single zoological survey in the Galápagos spanning 1 year in the late 1960s (Houvenaghel, 1978). This will be referred to hereafter as the topographic upwelling hypothesis.

Recently, new observations have emerged that appear to support the topographic upwelling hypothesis. A glider survey called Repeat Observations by Gliders in the Equatorial Region (ROGER; Rudnick et al., 2021) was sustained for three years (2013–2016), sampling along 93°W and diagonally to the southern and northern tips of Isla Isabela (Figure 1b). The ROGER gliders, equipped with Acoustic Doppler Current Profilers, quantified the horizontal volume transport budget west of the Galápagos, which enabled the calculation of vertical velocity by integration of the continuity equation. A local maximum in vertical velocity averaged within the ROGER sampling region of 1–2 m day^{-1} was found at a depth of 30 m (Jakoboski et al., 2020). While that estimate is not higher than previous observational estimates valid for the open ocean far from the islands (*e.g.*, Johnson et al., 2001), it is apparent from Figure 1 that the ROGER sampling pattern encompassed a substantially greater area than that of the cold and productive pool adjacent to the islands. Importantly, ROGER was only able to quantify the *average* upwelling velocity throughout the trapezoidal sampling area, which is of course critically dependent on the scale of the glider sampling pattern if the upwelling occurs at a spatial scale smaller than that of the sampling region. The true spatial scales of upwelling, the peak vertical velocities where upwelling is occurring, and how closely they align with the surface signals of reduced SST and enhanced chlorophyll, remain unknown.

The objective of this study is to determine whether the global Argo array of profiling floats is capable of resolving the subsurface signature of physical processes sustaining the cold (and productive) waters associated with equatorial islands. To the extent that it is, Argo measurements are then combined with a high-resolution ocean reanalysis to cross-validate the observations. The Argo and reanalysis data sets, including some details of their processing and analysis methods, are described in the following section. Results are presented in Section 3 and a summary and discussion are given in Section 4.

2. Data and Methods

The primary data source of data used in this study is Argo, a global array of profiling floats (Argo, 2000; Roemmich et al., 2009). The Argo array provides real-time measurements of the temperature, salinity, and pressure for the global ocean to a depth of approximately 2,000 m. Argo floats have been deployed since the early 2000s and reached the target coverage in 2007. Nearly 4,000 Argo floats are currently sampling the global ocean, providing a profile every 10 days. Scientific applications of the Argo array benefit from its global coverage with unprecedented spatial and temporal resolution, and generally negligible seasonal bias in sampling (Roemmich et al., 2009). For this study, the desired Argo profiles were retrieved from the Argovis database, using the Argovis application programming interface (API) for fast delivery, visualization, and analysis of Argo data (Tucker et al., 2020).

The vertical resolution of an Argo profile varies, but is generally between approximately 1–10 m (most commonly ~2 m) in the upper 100 m. To simplify visualization and calculation of statistics, such as spatial and temporal averages, all profiles were linearly interpolated to a common 1-m vertical grid from 5 to 500 m upon retrieval from Argovis. All Argo profiles between January 2000 and December 2021 were retrieved from two regions (Figures 2a and 2b): one in the vicinity of the Gilbert Islands, Republic of Kiribati (165°E–180°W, 5°S–5°N), and one in the vicinity of the Galápagos Islands, Republic of Ecuador (95°W–90°W, 3°S–2°N). The sampling density taken over 22 years is comparable between the two regions—approximately 80 profiles per square degree (Figures 2a and 2b). Lack of sampling to the southeast of Isla Isabela, Galápagos, is due to very shallow bathymetry on the Galápagos platform (<500 m); ocean depths to the immediate west of the Galápagos are very deep owing to extremely steep bathymetric slopes there (reaching 3.5 km depth within 12 km of the shoreline). Similar to the global Argo array itself, the sampling density increases over time and varies from year to year (Figures 2c and 2d), and is subject to negligible seasonal bias (Figures 2e and 2f). Given the strong influence of El

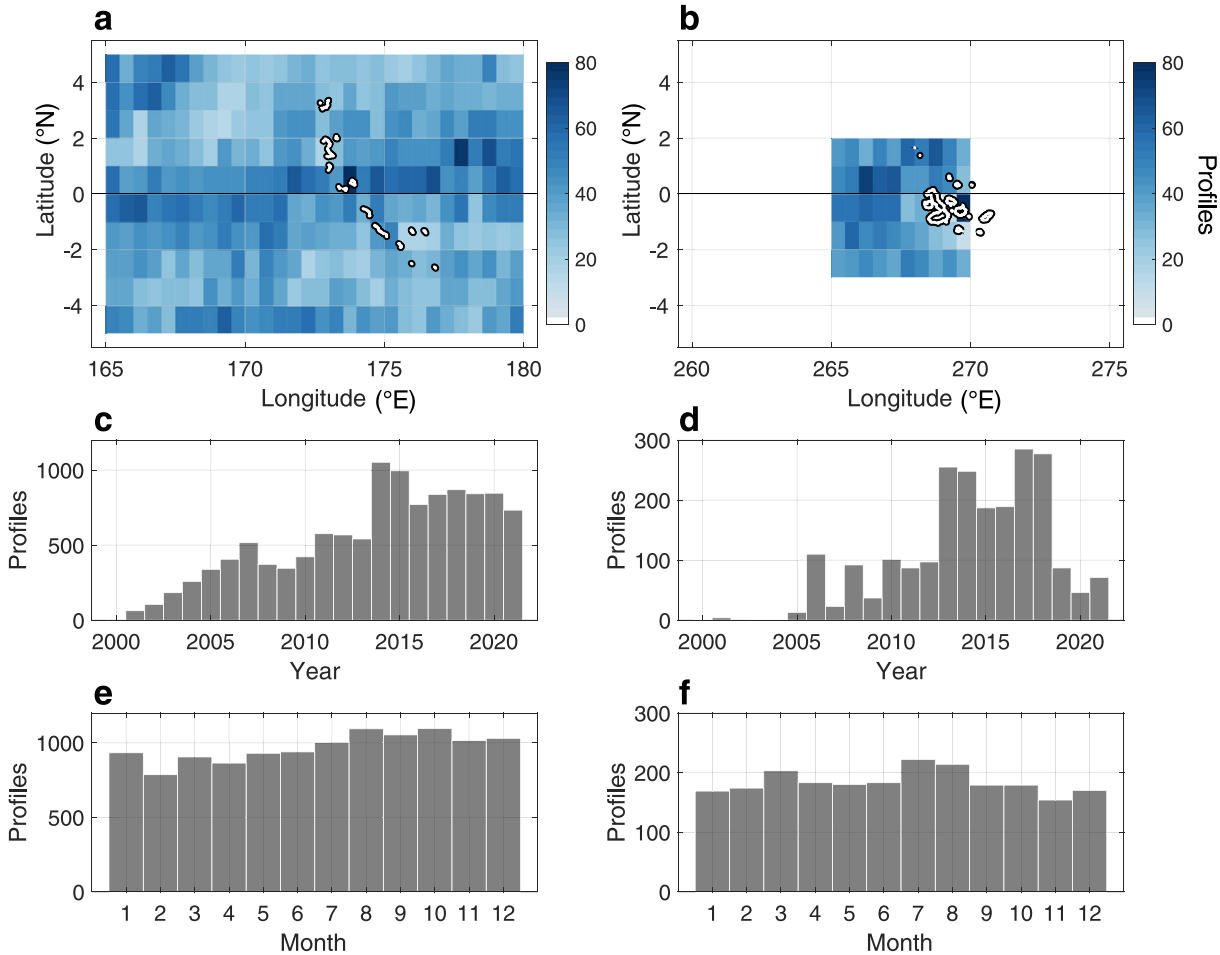

Figure 2. Spatial and temporal sampling of Argo. Number of Argo profiles in 0.5° longitude by 1° latitude bins in the vicinity of the (a) Gilbert and (b) Galápagos Islands during years 2000–2021. The number of profiles from each region per year (month) is given in panels (c–f).

Niño-Southern Oscillation (ENSO) on the equatorial circulation (*e.g.*, Firing et al., 1983; Rudnick et al., 2021), it is important to acknowledge the presence of interannual variability. Consideration of an ENSO index throughout the Argo era, however, suggests that 22 years of observations, particularly with relatively uniform seasonal sampling, are sufficient to adequately minimize the impact of ENSO on the mean calculations (Figure S1 in Supporting Information S1).

To cross-validate results from Argo and aid in their dynamical interpretation, the temperature and velocity fields from the GLobal Ocean ReanalYsis and Simulation (GLORYS)-12v1 product (Lellouche et al., 2018, 2021) are used. GLORYS-12v1 is a relatively new global ocean, eddy-resolving reanalysis covering the altimeter era at 1/12° (~9 km) horizontal resolution on 50 vertical levels. The ocean model component is the NEMO platform driven at the surface by the ERA5 reanalyzes for recent years. Oceanographic observations are assimilated by means of a reduced-order Kalman filter and 3D-VAR provides a correction for the slowly evolving large-scale biases in temperature and salinity. Along track altimetry, SST, sea ice concentration and in situ temperature, and salinity profiles are jointly assimilated. GLORYS-12v1 fields are currently available from 1993 to 2018; the temporal means calculated across the full period are used here. Unlike most coupled models and ocean state estimates/reanalyses, GLORYS-12v1 includes an exceptionally well-resolved Galápagos Archipelago and a mean zonal circulation just upstream (93°W) that validates very well against recent in situ observations (Figure S2 in Supporting Information S1). These two aspects of GLORYS-12v1 render it suitable to the present study, especially in the eastern equatorial Pacific. The Gilbert Islands consist of atolls of considerably smaller scale and are partially resolved by GLORYS-12v1, but not well. An ocean model resolution of 1/22° (~5 km) is likely necessary to accurately resolve their interaction with ocean circulation (Karnauskas et al., 2017).

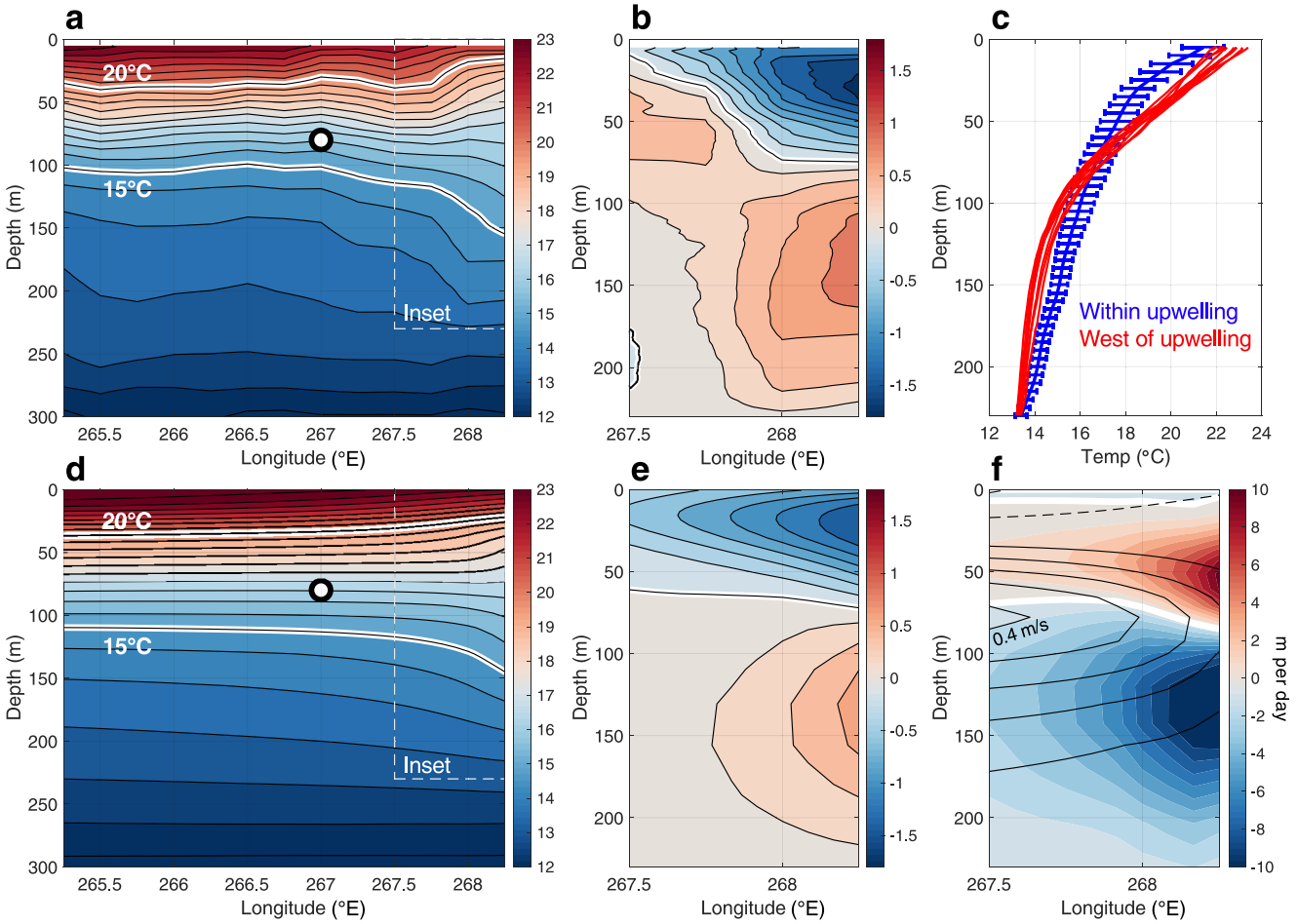

Figure 3. Subsurface temperature signals west of the Galápagos in Argo and a high-resolution ocean reanalysis. Cross section of Argo-measured temperature (contour interval 0.5°C) averaged from 1°S to 0°S in 0.5°-wide bins every 0.25° longitude west of the Galápagos Islands (a). The 15°C and 20°C isotherms are highlighted in white, the circular marker at 267°E, 80 m indicates the depth of the maximum zonal velocity of the equatorial undercurrent measured by the Repeat Observations by Gliders in the Equatorial Region glider campaign, and the dashed inset box indicates the domain displayed in panel (b). The westernmost Galápagos Islands are located at the eastern terminus of the plot. (b) As in panel (a) but expressed as anomalies relative to the zonal mean across the full domain of panel (a) (contour interval 0.2°C). Panel (c) shows each mean profile constituting the cross section (a) west of the easternmost bin ("west of upwelling," red lines). The easternmost mean profile ("within upwelling") is drawn in blue with 95% confidence intervals on the estimated mean at each depth (±2 standard errors). (d, e) As in panels (a, b) but as estimated by GLobal Ocean ReanalYsis and Simulation (GLORYS)-12v1; simple latitudinal averages taken at each longitude on the GLORYS-12v1 grid (rather than bins). Cross section of vertical velocity (color shading, interval 1 m day^{-1}) and zonal velocity (black contours, interval 0.1 m s^{-1}, zero omitted) averaged from 0.5°S to 0°S estimated by GLORYS-12v1 (f).

Insights are drawn from a few additional observational data sets in this study. Contextual maps of SST and surface chlorophyll-*a* concentration shown in Figure 1 are from the Moderate Resolution Imaging Spectroradiometer (MODIS) sensor on board the Terra (~2000–present) and Aqua (~2002–present) satellites (Esaias et al., 1998; Kilpatrick et al., 2015), using the 4-km resolution "entire mission composite" Level-3 processed (L3) products. For SST, a simple average of daytime and nighttime products is calculated to reduce the spatiotemporal noise and minimize instrument bias. For indication of the depth of the EUC core just upstream of the Galápagos (Figure 3), measurements along 93°W during the recent ROGER glider campaign are used (Rudnick et al., 2021). For the western Pacific (Figure 4), the climatology of Johnson et al. (2002) based on cruises throughout the 1990s is used; the linear interpolation between their mean sections at 165°E and 180°E is used to obtain an estimate at 172.5°E—just upstream of the Gilberts.

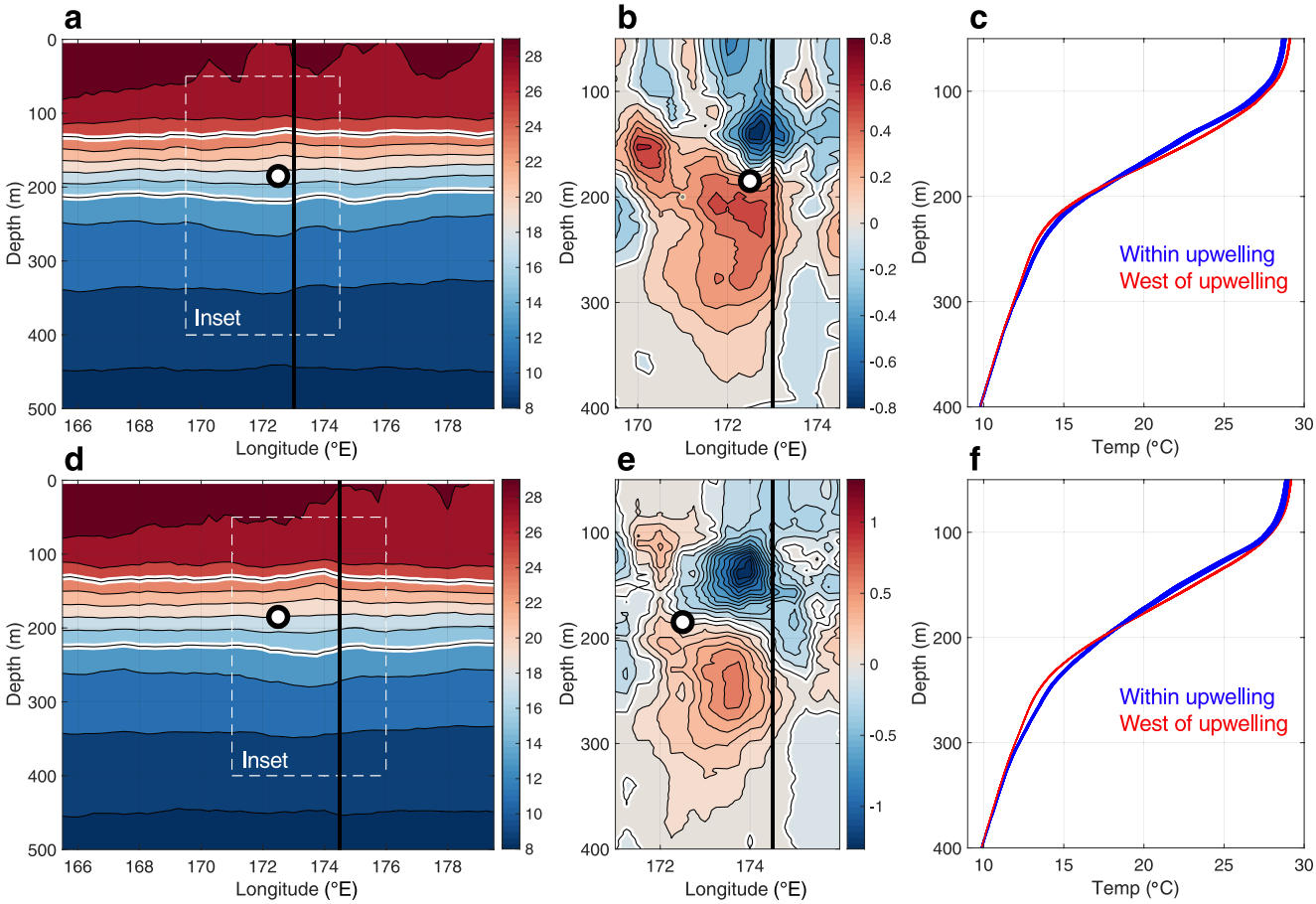

Figure 4. Argo temperature signals at the Gilberts. Cross section of Argo-measured temperature (contour interval 2°C) averaged from 0°N to 2°N in 1°-wide bins every 0.25° longitude in the vicinity of the *northern* Gilbert Islands (a). The 15 and 25°C isotherms are highlighted in white, the circular marker at 172.5°E, 185 m indicates the depth of the maximum zonal velocity of the equatorial undercurrent measured by Johnson et al. (2002), the vertical black line gives a general indication of where the islands are located, and the dashed inset box indicates the domain displayed in panel (b). (b) As in panel (a) but expressed as anomalies relative to the zonal mean across the full domain of panel (a) (contour interval 0.1°C). Panel (c) shows the mean of all profiles constituting the cross section (a) between 172°E and 173.5°E ("within upwelling," blue line) and all profiles west of 172°E ("west of upwelling," red line). The thicknesses of the red and blue lines denote 95% confidence intervals on the estimated mean at each depth (±2 standard errors). (d–f) As in panels (a–c) but for the *southern* Gilbert Islands (*i.e.*, averaged from 1.5°S to 0°S). Note that the Gilbert Islands form a roughly diagonal line such that the islands south of the equator are located slightly east of those north of the equator (Figure 1a); for panel (f), the "within upwelling" domain is defined as 172.5°E–174.5°E.

3. Results

West of the Galápagos, Argo reveals a coherent local anomaly in temperature stratification that intensifies approaching the islands (Figure 3a). Within the thermocline, isotherms are lifted by several tens of meters, and near the bottom of the thermocline, isotherms are similarly depressed. The thickness of the 15–20°C layer doubles from 70 to 140 m between 93°W and the island boundary approximately 140 km away. Interestingly, evidence of this thermostad approaching the Galápagos appears in a 1966 transect from a remarkable survey that took continuous temperature profiles along the equator with ∼8 m vertical resolution and approached within <50 km of the coast of Isla Isabela—crossing just east of 92°W (Christensen, 1971). Mapping the 15–20°C layer thickness in all Argo profiles from the region confirms that the thermostad is indeed concentrated alongside the islands—generally east of 92°W and between the southern and northern ends of Isabela (Figure S3 in Supporting Information S1). Taken relative to the zonal mean, the local subsurface temperature anomalies exceed ±1°C (Figure 3b), are centered around 75 m depth, and are generally constrained to the narrow corridor between 92°W and the islands.

Surprisingly, Argo is also able to resolve a very similar subsurface signal just west of the much smaller Gilbert Islands in the western Pacific (Figure 4). In this case, the temperature anomalies are about half the amplitude

(±0.5°C) and, like the local thermocline, are centered about a deeper depth. As with the Galápagos (Figure 3c), the mean of profiles immediately west of the Gilbert Islands is significantly different from the mean of those further west, both above and below the nodal depth, based on a two-sample *t*-test (Figures 4c and 4f). As with the Galápagos, the vertical divergence balancing the deceleration of the EUC upon encountering equatorial islands is comprised of vertical velocities in both directions. In all cases, the depth at which the vertically distributed temperature anomalies cross zero near the islands is also approximately the depth of the "core" (or maximum zonal velocity) of the EUC—that is, approximately 185 m just upstream of the Gilbert Islands (Johnson et al., 2002) and 80 m just upstream of the Galápagos (Rudnick et al., 2021). This result is consistent with the topographic upwelling hypothesis proposed for the Galápagos by Houvenaghel (1978), with dynamical underpinnings provided by Drazin (1961) and Hendry and Wunsch (1973).

As a means to explore these observed phenomena further and with fields unobtainable through pure observations, we first repeat the temperature calculations west of the Galápagos with the GLORYS-12v1 reanalysis (Figures 3d and 3e). The consistency between the Argo and reanalysis temperature sections is quite remarkable, but not unexpected since GLORYS-12v1 assimilates Argo measurements. Next, we examine equivalent GLORYS-12v1 sections portraying the circulation (zonal and vertical velocities). The EUC in the 0.5°S–0°S average appears approaching the island from the west at ∼0.4 m s^{-1}, with a strong vertical divergence of water away from the depth at which the EUC subsequently meets the islands (Figure 3f). By comparing a latitudinal section of vertical velocity in the open ocean sufficiently far from islands to one directly adjacent to the Galápagos (Figure S4 in Supporting Information S1), it is obvious that this upwelling (and downwelling) is topographically driven and is readily distinguishable from wind-driven upwelling (Ekman suction) both in magnitude and in spatial structure. GLORYS-12v1 yields a peak upwelling velocity averaged across the open equatorial ocean of 1.7 m day^{-1} (similar to the 1.6 m day^{-1} reported by Johnson et al. (2001) over the same longitude domain) compared to 8.6 m day^{-1} averaged from 92°W to the Galápagos.

Just above and below the intense upwelling and downwelling signals are the cold and warm temperature anomalies (relative to the zonal mean), respectively, which is unambiguously diagnostic of a key role for the vertical temperature advection and entrainment in the steady-state heat balance beneath the cold pools observed west of equatorial islands, such as the Galápagos. A crude calculation of the magnitude of this term at 50 m using $w = 10$ m day^{-1} and $T_z = 5°/100$ m yields a considerable cooling effect of −0.5°C per day from advection alone, which should be balanced by horizontal advection and surface fluxes. Importantly, the topographic upwelling extends across the base of the mixed layer, enabling it to influence SST directly (Figure S5 in Supporting Information S1). It is therefore quite clear why the waters in the west of the Galápagos and Gilbert Islands are so cool (and productive), even as compared to the already relatively cool and productive (for the tropics) waters of the cold tongue upon which they superimpose in observations.

4. Summary and Discussion

This study presented an analysis of 22 years of Argo measurements in the vicinity of the Galápagos and Gilbert Islands to understand the scales and provenance of equatorial island upwelling systems. The observations reveal couplets of opposite signed temperature anomalies, arising from equatorial islands blocking the EUC, which drives vertical divergence and hence vertical temperature advection at the thermocline. When the Argo calculations are repeated, but only including profiles taken during the "strong EUC" season of April–June (Johnson et al., 2002; Karnauskas et al., 2010) at some expense of sampling and signal over noise, the pattern of temperature anomalies is well-retained including their position relative to the EUC core depth, but with much higher amplitude signals including a 50% stronger cold anomaly above the EUC (not shown). This lends further support to the topographic upwelling hypothesis, indicating the vertical divergence scales with the velocity of the inbound EUC. Viewed at the surface, the result of this process is local minima in SST and maxima in chlorophyll concentration.

As these observed signatures are consistent at two very different equatorial archipelagos situated in two very different tropical regimes—one chain of small, low-lying atolls at the edge of a warm pool, and one a more continuous north-south boundary with prominent subaerial volcanoes reaching 1 km elevation and situated squarely within the cold tongue, this mechanism may be general to all equatorial islands regardless of their size or arrangement, so long as they are in the path of the EUC. Moreover, this mechanism is readily distinguishable from those governing the impact of off-equatorial islands on the ocean circulation, such as the Hawaiian Islands. There, it

is the wind that is blocked by the islands, generating couplets of positive and negative wind stress curl that can induce circulation anomalies (Xie et al., 2001), and hence the surface property anomalies tend to be offset along the wind-normal axis rather than directly aligned with the island boundaries as in the signals examined here.

While the Pacific Ocean was the focus of this study, the equatorial islands exist in the Indian and Atlantic Oceans as well. For example, the Maldives may have an impact on the circulation of the Indian Ocean, but research to date has emphasized their potential impact on wave propagation and surface jets (Cane & du Penhoat, 1982; Han, 2005; Han et al., 1999; Yoon, 1981). Using sparse measurements, Knox (1974) observed EUC stagnation upstream of the Maldives and thermocline thickening, similar to that at Jarvis Island in the Pacific discussed by Hendry and Wunsch (1973). Yet, satellite observations of the Maldives do not readily reveal systematic cold/productive pools akin to those found west of the Gilbert and Galápagos Islands (and Jarvis), possibly because the EUC in the Indian Ocean is transient and relatively weak (Knauss & Taft, 1964; Schott & McCreary, 2001), and other factors such as thermocline depth and stratification may be unsupportive of mixed layer impacts. Rather, there is a general enhancement of surface chlorophyll *around* the islands, resemblant of the so-called island mass effect first described by Doty and Oguri (1956) and implicated at other off-equatorial island archipelagos such as the Marquesas (Signorini et al., 1999) and French Polynesia (James et al., 2020). Interactions of the Atlantic EUC with São Tomé, roughly the size of a single atoll in the Gilbert Islands and located ∼240 km offshore of Africa, have only recently begun to be investigated but new model experiments suggest that it may have important impacts on the coastal circulation and environment in the Gulf of Guinea (Napolitano et al., 2021).

Efforts to quantify the open-ocean, wind-driven upwelling velocity in the equatorial Pacific intensified in the 1980s with Wyrtki (1981), yielding observational estimates ranging from as low as 0.3 m day^{-1} (Meinen et al., 2001) to as high as 2.0 m day^{-1} Weisberg and Qiao (2000) and a diagnostic model predicting 2.5 m day^{-1} (Bryden & Brady, 1985). There has been much discussion in the literature attempting to reconcile these varying estimates, which are often based on different time periods, different regions (longitudinally), and different meridional scales. Paradoxically, the upwelling velocity above the EUC from Jakoboski et al. (2020), 1.5 m day^{-1}, was well within the realm of those earlier estimates, despite being made very close to the coast of the Galápagos Islands where surface fields suggest that upwelling may be much stronger than in the open ocean. This paradox is resolved by considering the area of the ROGER sampling region relative to the spatial scale of the topographic upwelling signal residing within it, as inferred from Argo temperature anomalies and GLORYS-12v1 circulation fields. Consistent with Figure 3, the upwelling plume in contact with the western shores of the Galápagos Islands is considerably smaller than the area of the ROGER sampling region (Figure S6 in Supporting Information S1). The fraction of the sampling region with vertical velocity at least 1.5 m day^{-1} at 50 m is only 22%, and the upwelling rate within that smaller area locally reaches 12 m day^{-1}. Satisfyingly, the area-averaged vertical velocity at 50 m within the sampling region estimated by GLORYS-12v1 is 1.2 m day^{-1}, which is well within the uncertainty of the glider-based estimate by Jakoboski et al. (2020).

We should note that the results presented here, which support a topographic upwelling mechanism, do not preclude other processes from playing a role in maintaining the cool SST and/or high productivity observed west of equatorial islands. A recent modeling study by Forryan et al. (2021), for example, finds wind-driven submesoscale instabilities and circulations at shallower depths to play a key role in driving upwelling, and Jakoboski et al. (2022) recently used gliders to diagnose environmental conditions suitable for some key instabilities. It is possible that these various mechanisms are in fact complementary; the vertical advective cooling evident in our analysis is centered around 30 m depth, so the water entrained into the mixed layer by any turbulent mixing (wind-driven or otherwise) will be cooler as a result. The South Equatorial Current (the westward surface current) may also play an important role, particularly at the Gilbert Islands.

In a rapidly changing global ocean, especially in regions where compounding anthropogenic pressures are significant, a comprehensive understanding of regional ocean and climate dynamics is essential. The Argo array has been a driving force behind the revolution in observing and understanding the ocean, especially at large scales. It is characteristically challenging to use Argo to study regional-scale phenomena if one is interested in a mean state, given the sampling density problem. However, with the right combination of scales and signal over noise, and complementary data sets, there is great potential for regional applications—especially as the Argo array is sustained over multiple decades. On occasion, such resources give us insights into the ocean circulation beyond the prescient depictions by observationalists like Houvenaghel, Knauss, and Wyrtki who studied the eastern

equatorial Pacific several decades ago and without the luxury of global arrays, satellites, and state-of-the-art data assimilation systems.

Data Availability Statement

All data sets used in this study are freely and publicly available online and may be accessed directly as follows. Argo profiles via Argovis from https://argovis.colorado.edu/. GLORYS-12v1 reanalysis from https://resources.marine.copernicus.eu/product-detail/GLOBAL_MULTIYEAR_PHY_001_030/. MODIS SST and chlorophyll-a concentration from https://oceancolor.gsfc.nasa.gov/l3/. ROGER glider observations from https://doi.org/10.21238/S8SPRAY0090.

Acknowledgments
KBK acknowledges support from the National Science Foundation (award 1233282). DG acknowledges support from the National Science Foundation (award 1928305). The authors thank Dr. Eric Firing for helpful comments during review, as well as the Mercator Ocean Service Desk (Véronique Landes) and Dr. Aneesh Subramanian for assistance with acquiring GLORYS-12v1 vertical ocean velocity fields. Argo data are collected and made freely available by the International Argo Program and the national programs that contribute to it. The Argo Program is part of the Global Ocean Observing System.

References

Argo, G. D. A. C. (2000). Argo float data and metadata from Global Data Assembly Centre (Argo GDAC). *Seanoe*. https://doi.org/10.17882/42182

Bjerknes, J. (1969). Atmospheric teleconnections from the equatorial Pacific. *Monthly Weather Review*, *97*(3), 163–172. https://doi.org/10.1175/1520-0493(1969)097<0163:atftep>2.3.co;2

Bryden, H. L., & Brady, E. C. (1985). Diagnostic model of three-dimensional circulation in the upper equatorial Pacific Ocean. *Journal of Physical Oceanography*, *15*(10), 1255–1273. https://doi.org/10.1175/1520-0485(1985)015<1255:dmottd>2.0.co;2

Cane, M. A., & du Penhoat, Y. (1982). The effect of islands on low-frequency equatorial motions. *Journal of Marine Research*, *40*, 937–962.

Cannon, S. E., Aram, E., Beiateuea, T., Kiareti, A., Peter, M., & Donner, S. D. (2021). Coral reefs in the Gilbert Islands of Kiribati: Resistance, resilience, and recovery after more than a decade of multiple stressors. *PLoS One*, *16*(8), e0255304. https://doi.org/10.1371/journal.pone.0255304

Christensen, N., Jr. (1971). Observations of the Cromwell current near the Galápagos Islands. *Deep-Sea Research*, *18*(1), 27–33. https://doi.org/10.1016/0011-7471(71)90013-1

Cromwell, T. (1953). Circulation in a meridional plane in the central equatorial Pacific. *Journal of Marine Research*, *12*, 196–213.

Doty, M. S., & Oguri, M. (1956). The island mass effect. *ICES Journal of Marine Science*, *22*(1), 33–37. https://doi.org/10.1093/icesjms/22.1.33

Drazin, P. G. (1961). On the steady flow of a fluid of variable density past an obstacle. *Tellus*, *13*(2), 239–251. https://doi.org/10.3402/tellusa.v13i2.9451

Eden, C., & Timmermann, A. (2004). The influence of the Galápagos Islands on tropical temperatures, currents and the generation of tropical instability waves. *Geophysical Research Letters*, *31*(15), L15308. https://doi.org/10.1029/2004GL020060

Ekman, V. W. (1905). On the influence of the Earth's rotation on ocean-currents. *Arkiv for Matematik, Astronomi och Fysik*, *2*(11), 1–52.

Esaias, W. E., Abbott, M., Barton, I., Brown, O., Campbell, J., Carder, K., et al. (1998). An overview of MODIS capabilities for ocean science observations. *IEEE Transactions on Geoscience and Remote Sensing*, *36*(4), 1250–1265. https://doi.org/10.1109/36.701076

Feldman, G., Clark, D., & Halpern, D. (1984). Satellite ocean color observations of the phytoplankton distribution in the eastern equatorial Pacific during the 1982–1983 El Niño. *Science*, *226*(4678), 1069–1071. https://doi.org/10.1126/science.226.4678.1069

Field, C. B., Behrenfeld, M. J., Randerson, J. T., & Falkowski, P. (1998). Primary production of the biosphere: Integrating terrestrial and oceanic components. *Science*, *281*(5374), 237–240. https://doi.org/10.1126/science.281.5374.237

Firing, E., Lukas, R., Sadler, J., & Wyrtki, K. (1983). Equatorial undercurrent disappears during 1982–1983 El Niño. *Science*, *222*(4628), 1121–1123. https://doi.org/10.1126/science.222.4628.1121

Forryan, A., Naveira Garabato, A. C., Vic, C., Nurser, A. J. G., & Hearn, A. R. (2021). Galápagos upwelling driven by localized wind–front interactions. *Scientific Reports*, *11*(1), 1277. https://doi.org/10.1038/s41598-020-80609-2

Gove, J. M. (2005). *Upwelling variability at Jarvis island*, M. S. thesis, School of Ocean and Earth Science and Technology, University of Hawaii at Manoa.

Gove, J. M., Merrifield, M. A., & Brainard, R. E. (2006). Temporal variability of current-driven upwelling at Jarvis Island. *Journal of Geophysical Research*, *111*(C12), C12011. https://doi.org/10.1029/2005JC003161

Han, W., McCreary, J. P., Anderson, D. L. T., & Mariano, A. J. (1999). Dynamics of the eastward surface jets in the equatorial Indian Ocean. *Journal of Physical Oceanography*, *29*(9), 2191–2209. https://doi.org/10.1175/1520-0485(1999)029<2191:dotesj>2.0.co;2

Han, W. Q. (2005). Origins and dynamics of the 90-day and 30–60-day variations in the equatorial Indian Ocean. *Journal of Physical Oceanography*, *35*(5), 708–728. https://doi.org/10.1175/JPO2725.1

Hendry, R., & Wunsch, C. (1973). High Reynolds number flow past an equatorial island. *Journal of Fluid Mechanics*, *58*(1), 97–114. https://doi.org/10.1017/s0022112073002156

Houvenaghel, G. T. (1978). Oceanographic conditions in the Galapagos archipelago and their relationships with life on the islands. In R. Boje & M. Tomczak (Eds.), *Upwelling ecosystems* (pp. 181–200). Springer. Chapter 15.

Jakoboski, J., Todd, R. E., Owens, W. B., Karnauskas, K. B., & Rudnick, D. L. (2020). Bifurcation and upwelling of the equatorial undercurrent west of the Galápagos Archipelago. *Journal of Physical Oceanography*, *50*(4), 887–905. https://doi.org/10.1175/JPO-D-19-0110.1

Jakoboski, J., Todd, R. E., Owens, W. B., Karnauskas, K. B., & Rudnick, D. L. (2022). Potential vorticity and instability in the Pacific equatorial undercurrent west of the Galápagos Archipelago. *Journal of Physical Oceanography*. https://doi.org/10.1175/JPO-D-21-0124.1

James, A. K., Washburn, L., Gotschalk, C., Maritorena, S., Alldredge, A., Nelson, C. E., et al. (2020). An island mass effect resolved near Mo'orea, French Polynesia. *Frontiers in Marine Science*, *7*, 16. https://doi.org/10.3389/fmars.2020.00016

Johnson, G. C., McPhaden, M. J., & Firing, E. (2001). Equatorial Pacific Ocean horizontal velocity, divergence, and upwelling. *Journal of Physical Oceanography*, *31*(3), 839–849. https://doi.org/10.1175/1520-0485(2001)031<0839:epohvd>2.0.co;2

Johnson, G. C., Sloyan, B. M., Kessler, W. S., & McTaggart, K. E. (2002). Direct measurements of upper ocean currents and water properties across the tropical Pacific Ocean during the 1990s. *Progress in Oceanography*, *52*(1), 31–61. https://doi.org/10.1016/s0079-6611(02)00021-6

Karnauskas, K. B., & Cohen, A. L. (2012). Equatorial refuge amid tropical warming. *Nature Climate Change*, *2*(7), 530–534. https://doi.org/10.1038/nclimate1499

Karnauskas, K. B., Cohen, A. L., & Gove, J. M. (2016). Mitigation of coral reef warming across the central Pacific by the equatorial undercurrent: A past and future divide. *Scientific Reports*, *6*(1), 21213. https://doi.org/10.1038/srep21213

Karnauskas, K. B., Jenouvrier, S., Brown, C. W., & Murtugudde, R. (2015). Strong sea surface cooling in the eastern equatorial Pacific and implications for Galápagos Penguin conservation. *Geophysical Research Letters*, *42*(15), 6432–6437. https://doi.org/10.1002/2015GL064456

Karnauskas, K. B., Johnson, G. C., & Murtugudde, R. (2017). On the climate impacts of atolls in the central equatorial Pacific. *International Journal of Climatology*, *37*(1), 197–203. https://doi.org/10.1002/joc.4697

Karnauskas, K. B., Murtugudde, R., & Busalacchi, A. J. (2007). The effect of the Galápagos Islands on the equatorial Pacific cold tongue. *Journal of Physical Oceanography*, *37*(5), 1266–1281. https://doi.org/10.1175/JPO3048.1

Karnauskas, K. B., Murtugudde, R., & Busalacchi, A. J. (2008). The effect of the Galápagos Islands on ENSO in forced ocean and hybrid coupled models. *Journal of Physical Oceanography*, *38*(11), 2519–2534. https://doi.org/10.1175/2008JPO3848.1

Karnauskas, K. B., Murtugudde, R., & Busalacchi, A. J. (2010). Observing the Galápagos–EUC interaction: Insights and challenges. *Journal of Physical Oceanography*, *40*(12), 2768–2777. https://doi.org/10.1175/2010JPO4461.1

Kilpatrick, K. A., Podestá, G., Walsh, S., Williams, E., Halliwell, V., Szczodrak, M., et al. (2015). A decade of sea surface temperature from MODIS. *Remote Sensing of Environment*, *165*, 27–41. https://doi.org/10.1016/j.rse.2015.04.023

Knauss, J. A., & Taft, B. A. (1964). Equatorial undercurrent of the Indian Ocean. *Science*, *143*(3604), 354–356. https://doi.org/10.1126/science.143.3604.354

Knox, R. A. (1974). Reconnaissance of the Indian Ocean equatorial undercurrent near Addu Atoll. In *Deep sea research and oceanographic abstracts* (Vol. 21, No. (2). pp. 123–129). https://doi.org/10.1016/0011-7471(74)90069-2

Lellouche, J.-M., Eric, G., Romain, B. B., Gilles, G., Angelique, M., Marie, D., et al. (2021). The copernicus global 1/12° oceanic and sea ice GLORYS12 reanalysis. *Frontiers of Earth Science*, *9*, 698876. https://doi.org/10.3389/feart.2021.698876

Lellouche, J.-M., Greiner, E., Le Galloudec, O., Garric, G., Regnier, C., Drevillon, M., et al. (2018). Recent updates to the Copernicus Marine Service global ocean monitoring and forecasting real-time 1/12° high-resolution system. *Ocean Science*, *14*(5), 1093–1126. https://doi.org/10.5194/os-14-1093-2018

Meinen, C. S., McPhaden, M. J., Johnson, G. C., Meinen, C. S., McPhaden, M. J., & Johnson, G. C. (2001). Vertical velocities and transports in the equatorial Pacific during 1993–99. *Journal of Physical Oceanography*, *31*(11), 3230–3248. https://doi.org/10.1175/1520-0485(2001)031<3230:VVATIT>2.0.CO;2

Napolitano, D., Alory, G., Dadou, I., Morel, Y., Jouanno, J., & Morvan, G. (2021). Influence of the Gulf of Guinea islands on the Atlantic equatorial undercurrent circulation. Retrieved from https://hal.archives-ouvertes.fr/hal-03368393

Pauly, D., & Christensen, V. (1995). Primary production required to sustain global fisheries. *Nature*, *374*(6519), 255–257. https://doi.org/10.1038/374255a0

Roemmich, D., Johnson, G. C., Riser, S., Davis, R., Gilson, J., Owens, W. B., et al. (2009). The Argo Program: Observing the global ocean with profiling floats. *Oceanography*, *22*(2), 34–43. https://doi.org/10.5670/oceanog.2009.36

Rudnick, D. L., Owens, W. B., Johnston, T. M. S., Karnauskas, K. B., Jakoboski, J., & Todd, R. E. (2021). The equatorial current system west of the Galápagos Islands during the 2014–2016 El Niño as observed by underwater gliders. *Journal of Physical Oceanography*, *51*(1), 3–17. https://doi.org/10.1175/JPO-D-20-0064.1

Schott, F. A., & McCreary, J. P. (2001). The monsoon circulation of the Indian Ocean. *Progress in Oceanography*, *51*, 1–123. https://doi.org/10.1016/S0079-6611(01)00083-0

Signorini, S. R., McClain, C. R., & Dandonneau, Y. (1999). Mixing and phytoplankton bloom in the wake of the Marquesas Islands. *Geophysical Research Letters*, *26*(20), 3121–3124. https://doi.org/10.1029/1999gl010470

Tucker, T., Giglio, D., Scanderbeg, M., & Shen, S. S. P. (2020). Argovis: A Web application for fast delivery, visualization, and analysis of Argo data. *Journal of Atmospheric and Oceanic Technology*, *37*(3), 401–416. https://doi.org/10.1175/jtech-d-19-0041.1

Vargas, H., Lougheed, C., & Snell, H. (2005). Population size and trends of the Galápagos Penguin Spheniscus mendiculus. *Ibis*, *147*(2), 367–374. https://doi.org/10.1111/j.1474-919x.2005.00412.x

Weisberg, R. H., & Qiao, L. (2000). Equatorial upwelling in the central Pacific estimated from moored velocity profilers. *Journal of Physical Oceanography*, *30*(1), 105–124. https://doi.org/10.1175/1520-0485(2000)030<0105:euitcp>2.0.co;2

Wyrtki, K. (1981). An estimate of equatorial upwelling in the Pacific. *Journal of Physical Oceanography*, *11*(9), 1205–1214. https://doi.org/10.1175/1520-0485(1981)011<1205:aeoeui>2.0.co;2

Xie, S. P., Liu, W. T., Liu, Q., & Nonaka, M. (2001). Far-reaching effects of the Hawaiian Islands on the Pacific Ocean-atmosphere system. *Science*, *292*(5524), 2057–2060. https://doi.org/10.1126/science.1059781

Yoon, J.-H. (1981). Effects of islands on equatorial waves. *Journal of Geophysical Research*, *86*(C11), 10913–10920. https://doi.org/10.1029/jc086ic11p10913